

Morphology Control of Layer-Structured Gallium Selenide Nanowires

Hailin Peng,[†] Stefan Meister,[†] Candace K. Chan,[‡] Xiao Feng Zhang,[§] and Yi Cui^{*†}

Department of Materials Science and Engineering, Stanford University, Stanford, California 94305, Department of Chemistry, Stanford University, Stanford, California 94305, Electron Microscope Division, Hitachi High Technologies America, Inc., 5100 Franklin Drive, Pleasanton, California 94588

Received August 31, 2006; Revised Manuscript Received November 27, 2006

ABSTRACT

Layer-structured group III chalcogenides have highly anisotropic properties and are attractive materials for stable photocathodes and battery electrodes. We report the controlled synthesis and characterization of layer-structured GaSe nanowires via a catalyst-assisted vapor–liquid–solid (VLS) growth mechanism during GaSe powder evaporation. GaSe nanowires consist of Se–Ga–Ga–Se layers stacked together via van der Waals interactions to form belt-shaped nanowires with a growth direction along the [11–20], width along the [1–100], and height along the [0001] direction. Nanobelts exhibit a variety of morphologies including straight, zigzag, and saw-tooth shapes. These morphologies are realized by controlling the growth temperature and time so that the actual catalysts have a chemical composition of Au, Au–Ga alloy, or Ga. The participation of Ga in the VLS catalyst is important for achieving different morphologies of GaSe. In addition, GaSe nanotubes are also prepared by a slow growth process.

Layer-structured semiconductor materials such as group III monochalcogenides have highly anisotropic electrical, optical, and mechanical properties,¹ which result from the strong intralayer covalent bonding and the weak interlayer van der Waals interaction. The bonding anisotropy also suggests that there are no surface dangling bonds except at the edge of the layers and that photoexcited antibonding states do not weaken the metal–chalcogenide bond and enable the good photostability.² Their unique properties have made them attractive in applications such as solar cells³ and solid-state batteries.⁴ Their one-dimensional nanowire (NW) structures may afford better materials for these applications because NWs have a large surface area for charge carrier separation and for fast ion intercalation while maintaining efficient charge carrier transport.⁵ In addition, NWs can provide a good system for studying shape anisotropy together with size-dependent properties. However, a facile synthetic method to controllably produce group III monochalcogenide NWs has not been developed. Here we report the synthesis of GaSe NWs and show that NWs exhibit a variety of controllable morphologies including straight, zigzag, saw-tooth nanobelts (NBs), and nanotubes (NTs).

GaSe exhibits a hexagonal layered structure,⁶ with each layer consisting of Se–Ga–Ga–Se sheets. Each Ga atom

is tetragonally coordinated to three Se atoms and one Ga atom. Adjacent layers are held together by weaker van der Waals interactions. Disc-shaped GaSe quantum dots have been synthesized from organometallic precursors in an organic phase.⁷ GaSe NTs have been prepared recently by the evaporation of GaSe and the exfoliation with organics.⁸ Different from these previous studies, our synthesis of GaSe NWs is carried out through a vapor–liquid–solid (VLS) growth mechanism⁹ during GaSe thermal evaporation. The VLS mechanism has been used extensively for the growth of one-dimensional IV, II–VI, and III–V semiconductor nanostructures,¹⁰ in which Au nanoparticles function as universal catalysts. Inspired by this, we also use Au nanoparticles in our GaSe NW synthesis. The nanocatalyst compositions can be varied between pure Au, pure Ga, or a Au–Ga alloy by controlling the source and substrate temperature and growth time, also effectively controlling the morphologies of the resulting GaSe NWs.

The synthesis was conducted in a 12 in. horizontal tube furnace (Lindberg/Blue M) equipped with a 1 in. diameter quartz tube (Figure 1A). The source material, polycrystalline GaSe powder, was positioned in the middle of the furnace. The substrates, native-oxidized silicon (100) covered with 20 nm diameter Au particles, were placed downstream at the expected locations to accurately set the temperature. High-purity N₂ premixed with 2% H₂ (99.999%) acted as a carrier gas. The tube was pumped to a base pressure of 60 mTorr and flushed with the carrier gas repeatedly to decrease

* To whom correspondence should be addressed. E-mail: yicui@stanford.edu.

[†] Department of Materials Science and Engineering, Stanford University.

[‡] Department of Chemistry, Stanford University.

[§] Electron Microscope Division, Hitachi High Technologies America, Inc.

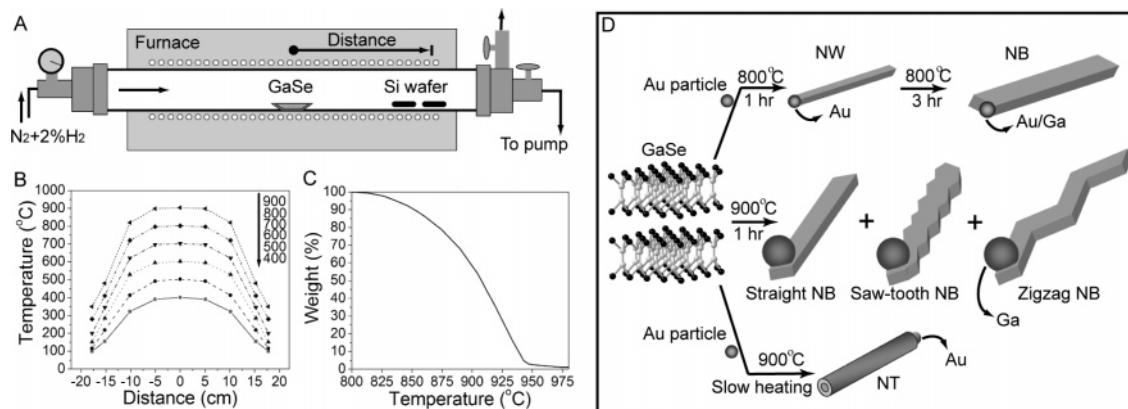


Figure 1. (A) Schematic diagram of the furnace used for the synthesis of GaSe nanostructures. (B) Temperature profile of the furnace at different set temperatures of 400, 500, 600, 700, 800, and 900 °C, respectively. (C) TG curve of bulk GaSe under dynamic vacuum (Adapted from ref 11). (D) Different morphologies of GaSe NWs controlled by growth temperature and time.

oxygen contamination. The carrier gas flow rate was maintained at 100 sccm at a pressure of 1 atm during the growth. The set temperature for the thermal evaporation was determined by the sublimation behavior of the source material. The thermogravimetry (TG) curve of GaSe under dynamic vacuum, adapted from ref 11 (Figure 1C),¹¹ indicates appreciable volatilization appears at about 800 °C and the complete evaporation is reached at about 950 °C. Therefore, the typical source temperature is ramped to 800 or 900 °C at a rate of 70 °C/min, and then maintained for 1 to 3 h. At the experimental temperature, GaSe sublimates congruently, and the vapor consists of predominantly Ga₂Se and Se₂ and a small amount of Ga₂.¹² The amount of Ga₂ in the vapor is a critical factor for different GaSe morphologies. The temperature distribution in the tube is important for controlling the morphologies of NWs and has been measured at different set temperatures (Figure 1B). A temperature gradient was established from the center to the end of the tube. The substrates were placed downstream at different temperature zones ranging from 600 to 400 °C. The morphology and structure of the synthesized nanomaterials were characterized using an FEI Sirion scanning electron microscope (SEM) and a Philips CM20 transmission electron microscope (TEM) operating at 200 kV. Chemical analysis was done using energy-dispersive X-ray spectrometers (EDX) equipped on the TEM and SEM. Different morphologies at different growth condition are summarized in Figure 1D and will be discussed below.

Figure 2A shows a typical SEM image of as-grown NWs after GaSe powder evaporation at 800 °C for 1 h. The NW widths range from 20 to 28 nm, and the lengths extend up to several microns. TEM observation provides structural information on the NWs. The TEM image of a single NW (Figure 2B) demonstrates that the NW is uniform (ca. 25 nm in width) and has a smooth surface along its length, with a particle (ca. 20 nm in diameter) at the tip. To confirm the chemical composition of the NW, EDX spectra were consecutively obtained from the wire part and the tip (Figure S1 in Supporting Information). The EDX analyses reveal the presence of Au in the tip, while the wire is GaSe with a Ga/Se atomic ratio of ~1.02, indicating that the composition of the NW is indeed GaSe. The selected-area electron

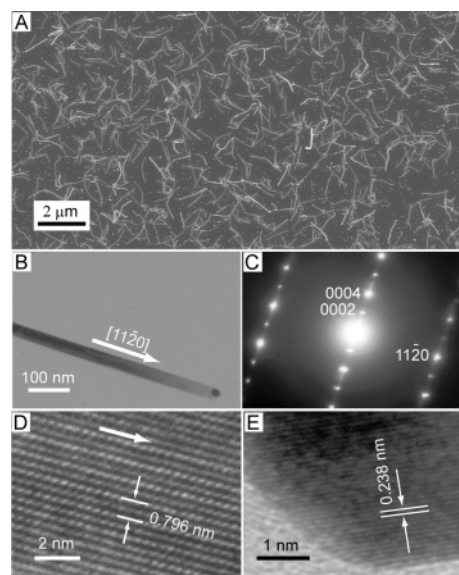


Figure 2. Nanowires grown at 800 °C for 1 h. (A) SEM image of as-grown NWs from GaSe evaporation. (B) Low-magnification TEM image of a single-crystalline hexagonal GaSe NW with a Au tip. (C) Selected-area electron diffraction pattern on GaSe NW in (B) indexed for the hexagonal structure with a¹¹⁻²⁰ growth direction. (D) HRTEM image of the same NW. The (0002) plane with a spacing of 0.796 nm is shown. The NW growth direction is indicated by the white arrow. (E) HRTEM image of the Au particle at the tip of the same NW. The lattice (111) plane of Au with a spacing of 0.238 nm is shown.

diffraction (SAED) pattern (Figure 2C) on the same NW shows a regular spot pattern, confirming the single-crystalline nature of the NW with a [11-20] growth direction. A high-resolution TEM (HRTEM) image (Figure 2D) of the same NW reveals that the lattice spacing of the planes parallel to the growth direction is 0.796 nm, agreeing well with the spacing of the (0002) planes of hexagonal GaSe. These results indicate that GaSe NWs consist of layers of Se-Ga-Ga-Se stacked together, as shown in Figure 1D. Extensive TEM studies on NWs with different zone axes aligned with the electron beam show that NWs all have similar widths. Due to the anisotropic nature of GaSe,¹ the information suggests that GaSe NWs have a nearly square-shaped cross section, i.e., the width and height are the same. The HRTEM

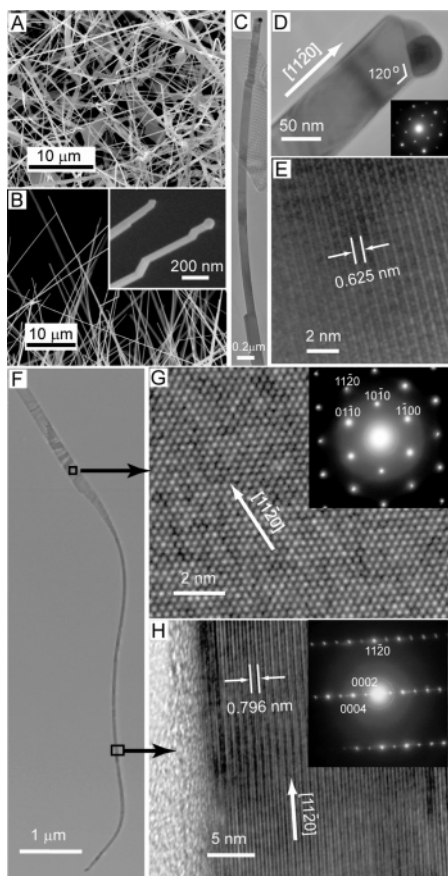


Figure 3. Nanowires grown at 800 °C for 3 h. (A) Representative SEM image of GaSe NWs over the substrate. (B) SEM image of the GaSe NWs at the edge of the substrate. Inset: close-up view highlighting the zigzag shape. (C,D) Low-magnification TEM image of a GaSe NB with a nanoparticle at the tip. Inset: corresponding SAED pattern. (E) HRTEM of the particle at the tip of the NB in (C,D). (F) Low-magnification TEM image of a GaSe NB that rotates 90° showing a top and side view. (G,H) HRTEM images of the same NB recorded from the boxed areas in (F), respectively. Insets represent the corresponding SAED patterns.

image of the tip shows lattice planes with a spacing of 0.238 nm, corresponding to those of the (111) plane of Au without any Ga or Se alloying (Figure 2E). The presence of the Au nanoparticle at the end of a NW corroborates the Au catalyst-assisted VLS growth mechanism.¹³ The diameter of the Au nanoparticle matches the width and height of the NWs, implying the possibility of size control by the catalyst size.

When extending the growth time to 3 h with the same source temperature of 800 °C, remarkable changes in the GaSe NW morphology can be identified compared to the NWs after 1 h growth (Figure 3). First, the NWs have a catalyst particle at the tip with a diameter of 40–50 nm, which is markedly bigger than the initial 20 nm Au particle (Figure 3D inset), implying the alloy formation in the catalyst. EDX spectra on the catalyst particle show the presence of both Au and Ga with a Au/Ga atomic ratio of 1.5, confirming Au–Ga alloy formation (Figure S2 in Supporting Information). The HRTEM image on the catalyst particle (Figure 3E) gives the lattice fringes of the particle as 0.625 nm, which does not match with Au or Ga, also suggesting the alloy formation. The incorporation of Ga in

3 h growth but not in 1 h growth is expected to originate from the slow thermal decomposition of GaSe at 800 °C. Control experiments at 800 °C without the Au nanoparticles did not yield any NW on the bare Si substrates, indicating that Au in nanoparticle catalyst is still the main ingredient to catalyze the growth of GaSe NWs at this temperature.

Second, the length of GaSe NWs is increased to tens of microns shown in SEMs of as-grown samples on the top and at the edge of substrate (Figure 3A and B, respectively). The width of the NWs is also increased significantly. Close to the catalyst tip, the width of NWs increases to 70–80 nm, which is approximately twice that of the catalyst alloy and approximately three times of that of NWs grown for 1 h. This suggests that the vapor–solid mechanism¹⁴ takes place during NW growth in addition to VLS growth. Due to its layered structure, a NW is expected to have many dangling bonds at the two edges, which can easily incorporate atoms directly coming from the gas phase or diffusing from the top/bottom surfaces. Indeed, we found that the width of some GaSe NWs is larger on the base side than on the tip side (Figure 3C), confirming the existence of a vapor–solid mechanism to increase the width of NWs.

Third, the height of NWs is much smaller than the width. Figure 3F shows a low-magnification TEM image of a GaSe NW that rotates 90°. Through the rotation, we can see a top and side view of a single NW. It has a height (50 nm) much smaller than the width (180 nm), revealing the NB shape. The flat surface of the NB is parallel to the (0002) plane, whereas its width is in the [1–100] direction. As shown in Figure 3G, the measured spacing of the planes is 0.323 nm, corresponding to the (10–10) lattice plane of hexagonal GaSe. The growth direction of the NB, as indicated by an arrow in Figure 3G, is [11–20], which is confirmed by the corresponding SAED pattern (Figure 3G inset). A HRTEM image of a NB taken from the side view shows the layered structure of GaSe (Figure 3H). The lattice image displays alternating bright and dark fringes that run parallel to the growth direction. The periodic spacing of these fringes is ~0.796 nm, as marked in the image, corresponding to the (0002) planes of hexagonal GaSe. The corresponding SAED pattern (Figure 3G inset) clearly indicates that the growth direction is [11–20], consistent with that obtained in the flat view. The height of GaSe NBs, which is [0001] layer stacking direction, is still similar to the size of Au–Ga alloyed catalyst. This suggests that the overgrowth on the height through a VS mechanism is much slower than at the edges because there are no dangling bonds on the layer surface.

These differences in the longer growth time at 800 °C appear to be attributed to the VLS overgrowth and the Au–Ga alloy catalyst. To further study how Ga affects the growth, we carried out the growth at 900 °C for 1 h because more Ga vapor can be produced during the faster decomposition of GaSe at higher temperature.^{11,12} A high yield of GaSe NBs is obtained, and an even more dramatic change of morphologies appears (Figure 1D). Large area SEM images show that there is a significant fraction of NBs with sawtooth (Figure 4A) and zigzag (Figure 4B) morphologies,

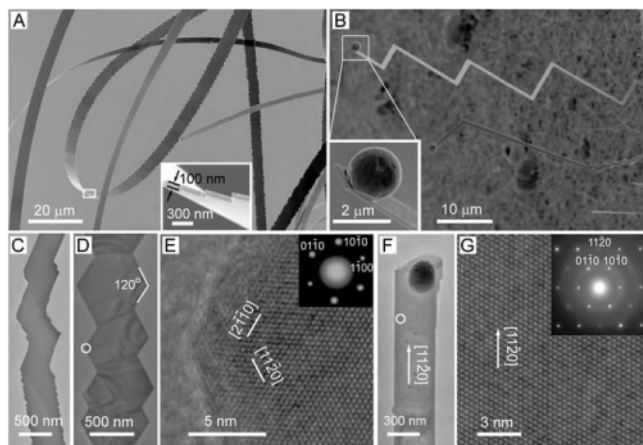


Figure 4. Nanowires grown at 900 °C for 1 h. (A) Representative SEM image of the GaSe NBs from GaSe evaporation at 900 °C. Inset: high-resolution SEM image of a selected area. (B) SEM image of zigzag NBs with a Ga sphere near the tip. Inset: higher magnification SEM image of the NB tip. (C) Low-magnification TEM of a straight-zigzag-sawtooth NB. (D) Low-magnification TEM image of a sawtooth NB. (E) HRTEM image recorded from the area indicated by the white circle in (D). Inset: the corresponding SAED pattern. (F) Low-magnification TEM image of a straight NB with a Ga sphere near the tip. (G) HRTEM image recorded from the area indicated by the white circle in (F). Inset: the corresponding SAED pattern of the NB tip.

which we can start to observe in a small fraction of NBs grown at 800 °C for 3 h (Figure 3B inset). The widths of the NBs become even larger, ranging from 200 nm to several microns, and lengths are up to several hundred microns. The thicknesses of the NBs are increased to ca. 100 nm (Figure 4A inset). Most interestingly, a large particle is located at or close to the NB tip, adhering to the flat side surface of the NB (Figure 4B and its inset), which is different from the VLS growth in most materials. In addition, NBs can be bent $>180^\circ$ without breaking, which suggests that the NBs are rather flexible in contrast to the fragile bulk crystal of GaSe (Figure 4A).¹⁵

To understand the structure characteristics of these different morphologies, we have conducted TEM studies. Low-magnification TEM observation (Figure 4C) reveals that sawtooth, zigzag, and straight structures can coexist in the same GaSe NB. As shown in Figure 4D, the NB with sawtooth-faceted sidewalls has an asymmetric configuration and an irregular periodicity. All sawtooth angles are uniformly 120° . Zigzag NBs also have the same 120° turning angle. This characteristic angle reflects the hexagonal symmetry of GaSe layered structures,¹ also suggesting sawtooth and zigzag are indeed the same morphology. Sawtooth structures can be understood as the small periodicity of zigzag structures. HRTEM observations and SAED patterns (Figure 4E) of the sawtooth indicate that the NB has a hexagonal structure with a zigzag growth direction along $[11\bar{2}0]$ and $[2\bar{1}\bar{1}0]$ successively. These two directions are equivalent, which is the same growth direction as the straight NBs grown at 800 °C. The SAED patterns do not change when the electron beam is moved along the length of NB, indicating that the whole NB is a single crystal. These data suggest that sawtooth, zigzag, and straight NBs at

different growth temperatures and times have an identical crystal structure and the same long-axis orientation.

EDX analysis in SEM reveals that the particle is solely composed of metallic Ga without Au (Figure S3 in Supporting Information). The TEM EDX spectrum on the catalyst particle close to the tip of NBs further confirms that the sphere consists of Ga without Au (Figure S3 in Supporting Information). Indeed, the growth without Au catalyst at 900 °C gives the same results, suggesting Ga is a more active catalyst for NB growth at this temperature. The SAED patterns focused on the catalyst show that the SAED spots that originate from the hexagonal GaSe NB. The diffuse rings in the SAED patterns suggest the amorphous nature of the Ga liquid droplets, which was also observed previously.¹⁶ The coexistence of both GaSe spots and Ga diffuse rings suggest that Ga particles and GaSe overlay on top of each other, consistent with the SEM observation.

We believe that the appearance of sawtooth and zigzag morphologies results from the participation of Ga as the catalyst. Ga liquid droplets have a low surface–interfacial energy compared to Au and their shape is much more sensitive to perturbation during growth,¹⁷ which causes the constant change in growth direction to make zigzag and sawtooth structures without increasing the free energy. Recently, anisotropic growth-induced sawtooth structures have been observed for wurtzite ZnO, ZnS, and CdSe,¹⁸ which is caused by the equilibrium crystal surface structure. Since Au-catalyzed GaSe NWs do not show sawtooth or zigzag morphologies, we conclude that this is less likely the explanation for the GaSe case. Periodic sawtooth faceting during VLS growth of Si NWs have also been directly observed,¹⁹ explained by periodic shrinking and expansion of the liquid droplet induced by the interplay of surface energy and geometry of NWs and the liquid droplet. This mechanism can explain the sawtooth patterns symmetric around the NW axis. The sawtooth and zigzag patterns in GaSe NBs do not have such a symmetric axis. We conclude that this mechanism alone is less likely to account for GaSe sawtooth and zigzag morphologies, but rather the mechanism is directly related to the probability to perturb the liquid droplet by the combination of surface–interfacial energy, thermal energy, gas flow, or other mechanical motions. Further studies are being carried out to understand these matters.

Layer-structured materials can in principle form NTs by rolling up the layers.^{8,20} Here we can produce GaSe NTs by slowly heating GaSe powder to 900 °C at a rate of 1 °C/min, which allows the Se–Ga–Ga–Se layers to have enough time to roll up. We note that we can find some fraction ($\sim 5\%$) of NTs, although the main product is still NBs. Figure 5A shows a TEM image of a GaSe NT. The NT is straight, with an inner diameter of ~ 20 nm and an outer diameter of ~ 35 nm. The HREM image of a wall of the NT (Figure 5B) gives a lattice spacing of ~ 0.8 nm, corresponding to the (0002) lattice planes of hexagonal GaSe. The NTs usually have a catalyst particle at one end and the other end is closed. The inner diameter is determined by the diameter of catalyst.

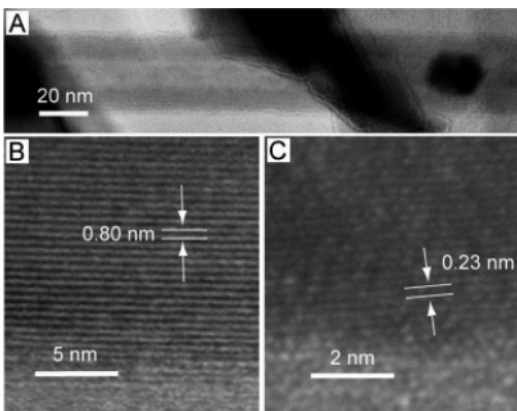


Figure 5. (A) TEM image of a GaSe NT. (B) HRTEM of a wall of the same NT. (C) HRTEM of the Au particle at the end of the same NT.

The HRTEM image of the particle (Figure 5C) shows the lattice spacing is ~ 0.23 nm, corresponding to the (111) plane spacing of Au. This suggests the GaSe NT is grown via a Au-assisted process.

In summary, GaSe NWs exhibit a variety of morphologies including straight, zigzag, saw-tooth NBs, and NTs (Figure 1D). We achieved control of these morphologies by tuning the actual chemical composition of catalysts with the growth temperature and time. GaSe NWs afford new materials for applications in solar cell and battery technology and for studying nanoscale properties with a high anisotropy in structure and shape.

Acknowledgment. Y.C. acknowledges support from Stanford New Faculty Startup Fund, CIS, and CPN seed fund. C.K.C. acknowledges support from a NSF Graduate Fellowship and Stanford Graduate Fellowship.

Supporting Information Available: Synthesis of the source precursor GaSe, the EDX spectra of GaSe NWs and NBs. This material is available free of charge via the Internet at <http://pubs.acs.org>.

References

- (1) Ferneliuss, N. C. *Prog. Cryst. Growth Charact.* **1994**, *28*, 275.
- (2) (a) *Solar Energy Conversion*; Seraphin, B. O., Ed.; Springer-Verlag: Berlin, 1979, Vol. 31. (b) Coehoorn, R.; Haas, C.; Dijkstra, J.; Flipse, C. J. F.; deGroot, R. A.; Wold, A. *Phys. Rev. B* **1987**, *35*, 6195.

- (3) (a) Afzaal, M.; O'Brien, P. *J. Mater. Chem* **2006**, *16*, 1597. (b) Qasrawi, A. F. *Semicond. Sci. Technol.* **2006**, *21*, 794. (c) Bernede, J. C.; Barreau, N.; Marsillac, S.; Assmann, L. *Appl. Surf. Sci.* **2002**, *195*, 222. (d) Djessas, K.; Yapi, S.; Masse, G.; Ibannain, M.; Gauffier, J. L. *J. Appl. Phys.* **2004**, *95*, 4111.
- (4) (a) Gomes da Costa, P.; Balkanski, M.; Wallis, R. F. *Phys. Rev. B* **1991**, *43*, 7066. (b) Julien, C.; Hatzikraniotis, E.; Paraskevopoulos, K. M.; Chevy, A.; Balkanski, M. *Solid State Ionics* **1986**, *859*, 18. (c) Kunc, K.; Zeyher, R. *Europhys. Lett.* **1988**, *7*, 611.
- (5) (a) Law, M.; Greene, L. E.; Johnson, J. C.; Saykally, R.; Yang, P. *Nat. Mater.* **2005**, *4*, 455. (b) Arico, A. S.; Bruce, P.; Scrosati, B.; Tarascon, J. M.; van Schalkwijk, W. *Nat. Mater.* **2005**, *4*, 366.
- (6) Levy, F. *Crystallography and Crystal Chemistry of Materials with Layered Structures*; Reidel: Holland, 1976.
- (7) (a) Chikan, V.; Kelley, D. F. *Nano Lett.* **2002**, *2*, 141. (b) Chikan, V.; Kelley, D. F. *Nano Lett.* **2002**, *2*, 1015. (c) Tu, H.; Yang, S.; Chikan, V.; Kelley, D. F. *J. Phys. Chem. B* **2004**, *108*, 4701. (d) Tu, H.; Mogyorosi, K.; Kelley, D. F. *Phys. Rev. B* **2005**, *72*, 205306. (e) Tu, H.; Kelley, D. F. *Nano Lett.* **2006**, *6*, 116.
- (8) Gautam, U. K.; Vivekchand, S. R. C.; Govindaraj, A.; Kulkarni, G. U.; Selvi, N. R.; Rao, C. N. R. *J. Am. Chem. Soc.* **2005**, *127*, 3658.
- (9) Wagner, R. S.; Ellis, W. C. *Appl. Phys. Lett.* **1964**, *4*, 89.
- (10) (a) Lieber, C. M. *MRS Bull.* **2003**, *28*, 486. (b) Yang, P. *MRS Bull.* **2005**, *30*, 85. (c) Björk, M. T.; Ohlsson, B. J.; Sass, T.; Persson, A. I.; Thelander, C.; Magnusson, M. H.; Deppert, K.; Wallenberg, L. R.; Samuelson, L. *Appl. Phys. Lett.* **2002**, *80*, 1058.
- (11) Wadsten, T. *Thermochim. Acta.* **1979**, *29*, 261.
- (12) (a) Ludviksson, A.; Rumaner, L. E.; Rogers, J. W.; Ohuchi, F. S. *J. Cryst. Growth* **1995**, *151*, 114. (b) Viswanathan, R.; Edwards, J. G. *J. Phys. Chem. B* **1998**, *102*, 2419.
- (13) Hu, J.; Odom, T. W.; Lieber, C. M. *Acc. Chem. Res.* **1999**, *32*, 435.
- (14) (a) Sears, G. W. *Acta Metall.* **1955**, *4*, 367. (b) Yang, P.; Lieber, C. M. *J. Mater. Res.* **1997**, *12*, 2981. (d) Pan, Z. W.; Dai, Z. R.; Wang, Z. L. *Science* **2001**, *291*, 1947.
- (15) (a) Balyts'kyi, O. O. *Mater. Sci.* **2003**, *39*, 561. (b) Mosca, D. H.; Mattoso, N.; Lepienski, C. M.; Veiga, W.; Mazzaro, I.; Etgens, V. H.; Eddrief, M. *J. Appl. Phys.* **2002**, *91*, 140.
- (16) Hu, J.; Bando, Y.; Zhan, J.; Golberg, D. *Adv. Mater.* **2005**, *17*, 1964.
- (17) (a) Kolevzon, V.; Gerbeth, G. *J. Phys. D: Appl. Phys.* **1996**, *29*, 2071. (b) Egry, I.; Lohoefer, G.; Jacobs, G. *Phys. Rev. Lett.* **1995**, *75*, 4043.
- (18) (a) Wang, Z. L.; Kong, X. Y.; Zuo, J. M. *Phys. Rev. Lett.* **2003**, *91*, 185502. (b) Moore, D.; Ronning, C.; Ma, C.; Wang, Z. L. *Chem. Phys. Lett.* **2004**, *385*, 8. (c) Ma, C.; Ding, Y.; Moore, D.; Wang, X. D.; Wang, Z. L. *J. Am. Chem. Soc.* **2004**, *126*, 708. (d) Ma, C.; Ding, Y.; Moore, D.; Wang, X. D.; Wang, Z. L. *Nature* **2004**, *427*, 497.
- (19) Ross, F. M.; Tersoff, J.; Reuter, M. C. *Phys. Rev. Lett.* **2005**, *95*, 146104.
- (20) (a) Iijima, S. *Nature* **1991**, *354*, 56. (b) Chopra, N. G.; Luyren, R. J.; Cherry, K.; Crespi, V. H.; Cohen, M. L.; Louie, S. G.; Zettl, A. *Science* **1995**, *269*, 966. (c) Côté, M.; Cohen, M. L. *Phys. Rev. B* **1998**, *58*, R4277. (d) Hollingsworth, J. A.; Poojary, D. M.; Clearfield, A.; Buhro, W. E. *J. Am. Chem. Soc.* **2000**, *122*, 3562. (e) Hu, P. A.; Liu, Y. Q.; Fu, L.; Cao, L. C.; Zhu, D. B. *Appl. Phys. A* **2005**, *80*, 1413. (f) Hu, J. Q.; Bando, Y.; Zhan, J. H.; Liu, Z. W.; Golberg, D. *Appl. Phys. Lett.* **2005**, *87*, 153112. (g) Feldman, Y.; Wasserman, E.; Srolovitz, D. J.; Tenne, R. *Science* **1995**, *267*, 222. (h) Tenne, R.; Margulis, L.; Genut, M.; Hodes, G. *Nature* **1992**, *360*, 444.

NL062047+